Cerebral Cortex Advance Access published August 12, 2014
Cerebral Cortex
doi:10.1093/cercor/bhu172

Brain Circuitry Supporting Multi-Organ Autonomic Outflow in Response to Nausea

Roberta Sclocco[1,2,3], Jieun Kim[1], Ronald G. Garcia[1,5], James D. Sheehan[4], Florian Beissner[1], Anna M. Bianchi[2], Sergio Cerutti[2], Braden Kuo[4], Riccardo Barbieri[3,†] and Vitaly Napadow[1,6,†]

[1]Department of Radiology, Martinos Center for Biomedical Imaging, Massachusetts General Hospital, Charlestown, MA, USA, [2]Department of Electronics, Information and Bioengineering, Politecnico di Milano, Milano, Italy, [3]Department of Anesthesia, Critical Care and Pain Medicine, Massachusetts General Hospital, Harvard Medical School, Boston, MA, USA, [4]Gastroenterology Unit, Massachusetts General Hospital, Harvard Medical School, Boston, MA, USA, [5]Medical School, Universidad de Santander (UDES), Bucaramanga, Colombia and [6]Department of Biomedical Engineering, Kyunghee University, Yongin, Korea

Address correspondence to Roberta Sclocco, Department of Electronics, Information and Bioengineering (DEIB), Politecnico di Milano, Via Golgi 39, 20133, Milano, Italy. Email: roberta.sclocco@polimi.it

[†]Riccardo Barbieri and Vitaly Napadow contributed equally to this publication.

While autonomic outflow is an important co-factor of nausea physiology, central control of this outflow is poorly understood. We evaluated sympathetic (skin conductance level) and cardiovagal (high-frequency heart rate variability) modulation, collected synchronously with functional MRI (fMRI) data during nauseogenic visual stimulation aimed to induce vection in susceptible individuals. Autonomic data guided analysis of neuroimaging data, using a stimulus-based (analysis windows set by visual stimulation protocol) and percept-based (windows set by subjects' ratings) approach. Increased sympathetic and decreased parasympathetic modulation was associated with robust and anti-correlated brain activity in response to nausea. Specifically, greater autonomic response was associated with reduced fMRI signal in brain regions such as the insula, suggesting an inhibitory relationship with premotor brainstem nuclei. Interestingly, some sympathetic/parasympathetic specificity was noted. Activity in default mode network and visual motion areas was anti-correlated with parasympathetic outflow at peak nausea. In contrast, lateral prefrontal cortical activity was anti-correlated with sympathetic outflow during recovery, soon after cessation of nauseogenic stimulation. These results suggest divergent central autonomic control for sympathetic and parasympathetic response to nausea. Autonomic outflow and the central autonomic network underlying ANS response to nausea may be an important determinant of overall nausea intensity and, ultimately, a potential therapeutic target.

Keywords: brain–gut interactions, motion sickness, neuroimaging, parasympathetic, sympathetic

Introduction

Nausea is a commonly experienced and distressing symptom of multiple disorders. Despite the large inter- and intra-subject differences in the autonomic response pattern reported in the literature (Graybiel and Lackner 1980; Mullen et al. 1998; Muth 2006), nausea elicits robust modulation of autonomic nervous system (ANS) outflow (Cowings et al. 1986; Doweck et al. 1997; LaCount et al. 2011; Muth 2006; Ohyama et al. 2007). Specifically, Muth stated in his review that, despite the early controversy about the importance of ANS to motion sickness, "it is irrefutable that the physiological expression of motion sickness is characterized by an autonomic-gastrointestinal cascade" (Muth 2006). Such ANS outflow involves both the sympathetic and parasympathetic branches, as evidenced in our recent study (LaCount et al. 2011). However, the brain's central autonomic network mobilized by nausea is currently unknown. This network is comprised of brain regions that control peripheral ANS outflow, as well as regions that sense this peripheral ANS activity. Vagal afference is thought to trigger nausea sensation, particularly for gastrointestinal derived nausea (Stern et al. 2011). Such afference may also sensitize feedback circuits along this nerve, contributing to the robust ANS outflow noted as a common physiological co-factor of this aversive sensation. In fact, perception of autonomic-associated sensations (e.g. sweating, stomach awareness, and increased salivation) is commonly included in nausea rating questionnaires (Muth et al. 1996). Importantly, nausea-associated ANS outflow may also serve to amplify other nausea sensations (e.g. dizziness, fatigue, and vertigo) via feedback to expectancy and memory brain circuitries, as expectations are known to strongly modulate nausea sensation (Levine et al. 2006). Thus, autonomic outflow and the central autonomic network underlying ANS response to nausea may be an important determinant of overall nausea intensity and, ultimately, a potential therapeutic target.

Previous studies reported differing interpretations regarding the modulation of the 2 ANS branches due to motion sickness and whether sympathetic or parasympathetic modulation was more dominant. For example, Doweck et al. (1997) argued that inter-beat intervals (R–R) spectral changes showed a decrease in parasympathetic activity, whereas Ohyama et al. (2007) interpreted heart rate (HR) spectral changes as an increase in sympathetic with no change in parasympathetic activity. Moreover, Ishii et al. (1987) expressed HR variations as the coefficient of variance of mean R–R interval; the authors found that the increase of this index in sickness was blocked by parasympathetic muscarinic agonist atropine, but not by propranolol, and argued for vagal parasympathetic downregulation. While these contrasting results reflect the difficulty of attributing motion sickness to the unique modulation of either sympathetic ("fight of flight") or parasympathetic ("rest and relax") autonomic responses (Sheehan et al. 2011), recent studies have clearly shown that ANS response during nausea spans multiple end-organs and is consistent with upregulation of sympathetic and downregulation of parasympathetic outflow (LaCount et al. 2011; Muth 2006).

While few neuroimaging studies have investigated the brain circuitry supporting nausea, our recent functional MRI (fMRI) study suggested that phasic activations, which precipitate nausea ratings increases, mainly involved brainstem and limbic regions, whereas sustained activation following such increases revealed a more widespread activity, encompassing interoceptive, limbic, somatosensory, and cognitive networks, thus highlighting the multi-dimensional complexity of nausea (Napadow et al. 2013).

Evaluation of the central autonomic network supporting ANS outflow during nausea requires a combined ANS/fMRI approach, where measures of ANS outflow can be used to guide fMRI data analysis. In recent years, a growing number of studies have investigated the role of different cortical, subcortical, and brainstem regions in autonomic control during a variety of different tasks and sensory stimuli, and our recent neuroimaging meta-analysis has summarized the diversity of brain regions supporting differential control of this human central autonomic network (Beissner et al. 2013). For example, while the amygdala, insula, and mid-cingulate cortices were found to form the core of the central autonomic network, regional specificity was found when comparing sympathetic and parasympathetic control networks, as well as when comparing central autonomic response with different tasks and stimuli. However, despite the large number of tasks and stimuli that have been studied with different combined ANS/fMRI methods, nausea has not been explored and the neural correlates of sympathetic and parasympathetic modulation during nausea have, to our knowledge, never been evaluated.

Our approach evaluated sympathetic and cardiovagal modulation, by means of skin conductance level (SCL), HR, and the high-frequency component of the Heart Rate variability (HRV) power spectrum (HF-HRV). These autonomic data were collected synchronously with fMRI data during nauseogenic visual stimulation aimed to induce motion sickness in susceptible individuals. We used both a stimulus-based analysis and a percept-based analysis, allowing for different methodological approaches to characterize the central autonomic network supporting nausea. We hypothesized that brain activity in visual motion areas such as MT+/V5, as well as previously noted central autonomic network regions such as the insula and cingulate, would be specifically linked with ANS outflow due to motion sickness-induced nausea.

Methods

Subjects

Right-handed [Edinburgh Inventory (Oldfield 1971)] subjects were recruited through advertisement and prescreened for increased susceptibility to motion sickness, as indicated by a score of >60 on the Motion Sickness Susceptibility Questionnaire [MSSQ (Golding 1998)]. Subjects were confirmed for motion sickness susceptibility during a mock MRI behavioral session in which they rated the intensity of nausea developed when exposed to a nauseogenic stimulus (see below). Subjects scoring >60 on the MSSQ but reporting <2 on a scale from 0 to 4 (see below) in response to the nauseogenic stimulus were excluded. Seventeen subjects (all female, age: 28.4 ± 8.5 years, mean ± SD) met both criteria and were asked to continue on to the MRI experimental session. A cohort of 8 subjects (all female, age: 25 ± 1.1 years), not showing susceptibility to motion sickness (MSSQ < 60, rating < 2 in the mock MRI behavioral session), underwent the same experimental session to serve as controls. Subjects also had no history of vestibular or balance disorders, as confirmed by clinician (BK) prior to any testing, nor did they need corrective vision or, if they did, were allowed to wear their contact lenses.

Subjects were instructed to abstain from food and water for 12 h and from cigarettes and alcohol for 24 h prior to fMRI. This was deemed necessary for safety reasons, as subjects would be stimulated to the verge of vomiting. All experiments took place between 7 AM and 12 PM at the Martinos Center for Biomedical Imaging in Charlestown, MA. Written informed consent was obtained from all participants, and the protocol was approved by the Human Research Committee of Massachusetts General Hospital.

Experimental Protocol

Subjects were placed, supine, in a 1.5 T Siemens Avanto MRI scanner (Siemens Medical Systems). A specialized 23-channel head coil constructed at the Martinos Center for Biomedical Imaging (Wiggins et al. 2006) was used to allow for a large, unimpeded field-of-view, critical for inducing motion sickness with visual stimuli. The stimulus was delivered by projection from the rear onto a concave screen with a central section (30.48 cm wide, 40.64 cm high), and 2 side wings (10.16 cm wide, semicircular) inclined at 45° relative to the central section. This screen was positioned approximately 10 cm in front of their eyes. Thus, assuming a single central view point, the field of view was 165.7°, covering both central and peripheral fields.

After an initial 5-min baseline period during which the subjects were asked to lie still and stare directly ahead at a crosshair projected onto the center of the screen, the nauseogenic visual stimulus was presented, consisting of an alternation of black and white stripes (black stripes 1.2 cm, 6.9° viewing angle; white stripes 1.85 cm, 10.6° viewing angle) with left-to-right circular motion at 62.5°/s. Because of this left-to-right horizontal translation, a vection sensation is induced in the subjects, who therefore experience a false sensation of translating or rotating to their left. The maximum duration of this nauseogenic stimulus was fixed at 20 min, but the subjects were able to interrupt it anytime by button press when they reached a predetermined maximum level of discomfort (see below); the experimental procedure ended with a second 5-min period of crosshair fixation.

During and after the nauseogenic visual stripes stimulation, subjects used a button box to freely (without cues) rate their overall nausea level ranging from "0" to "4." These ratings were verbally instructed and practiced during the behavioral session, and subjects were instructed that a rating of "0" indicated no nausea, a rating of "1" indicated "mild" nausea, a level of "2" indicated "moderate" nausea, and a rating of "3" indicated "strong" nausea sensation. If they reached a rating of "4," indicating "severe" nausea with the impending urge to vomit if the stimulus continues according to their past experience, the stimulus would be terminated (Fig. 1).

Physiological Monitoring

All peripheral autonomic physiological signals were collected at 400 Hz using Chart Data Acquisition Software (ADInstruments) on a laptop equipped with a 16-channel Powerlab DAQ System (ADInstruments). Skin conductance level was measured with MRI-compatible bipolar Ag/AgCl finger electrodes (MLT117F, ADInstruments) placed on the palmar aspect of the second and fourth fingers of the nondominant (left) hand, prior to the MRI session. Subjects' electrocardiogram (ECG) signal was collected with an MRI-compatible Patient Monitoring system (Model 3150, Invivo Research, Inc.) through MRI-compatible electrodes (VerMed, Bellows Falls) placed on the chest. Of the original cohort of 17 nausea-prone subjects and 8 controls, 1 nausea-prone subject was excluded from all the analyses due to low-quality ANS signals; 6 additional nausea-prone subjects and 3 controls showed a low-quality SCL signal and were excluded. Thus, the parasympathetic-related analysis was performed on 16 nausea-prone subjects and 8 controls, whereas the sympathetic-related analysis was performed on 11 nausea-prone subjects and 5 controls.

MRI Data Collection

Concurrently with autonomic monitoring, whole-brain blood oxygen level-dependent (BOLD) fMRI data were collected, using a gradient echo T_2^*-weighted pulse sequence (repetition time [TR]/echo time [TE] = 3 s/30 ms, slice thickness = 3.0 mm, interslice gap = 0.6 mm, matrix = 64 × 64, FOV = 200 mm, flip angle [FA] = 90°). The fMRI images were collected continuously during the baseline, stimulus, and recovery periods, resulting in a maximum of 600 continuously collected volumes when the visual stimulation was not interrupted by the subject reaching severe nausea sensation. In order to facilitate group analyses and localization, high-resolution T_1-weighted structural imaging was also completed, prior to fMRI scanning, using a standard MPRAGE pulse sequence (TR/TE/TI = 2730/3.39/1000 ms, slice thickness = 1.33 mm, FOV = 156 mm, FA = 7°).

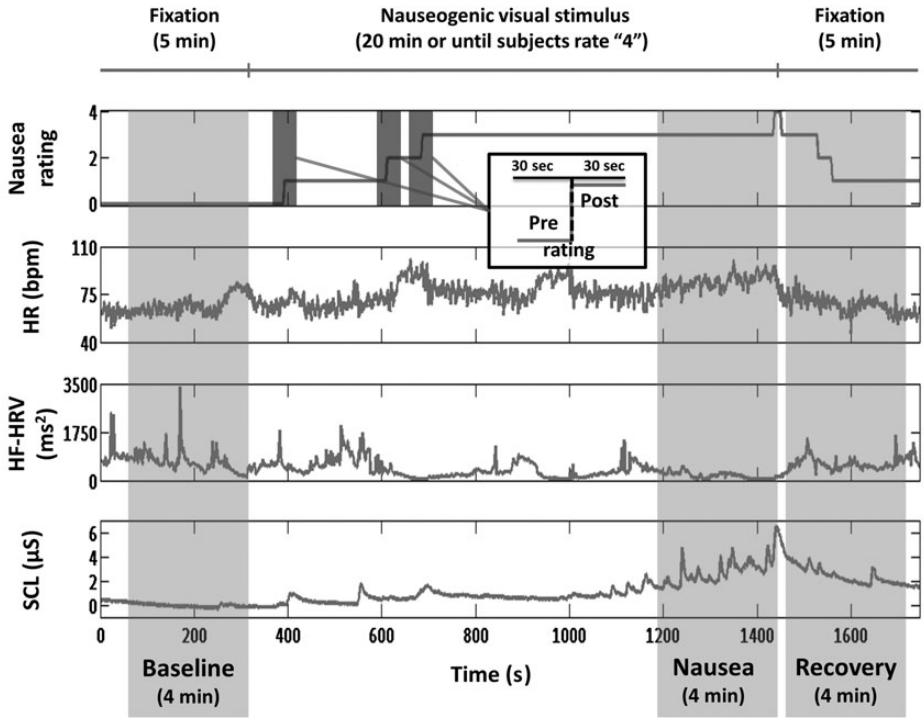

Figure 1. Experimental protocol design, window definition, nausea ratings, and autonomic signals from a representative subject. A stimulus-based analysis evaluated autonomic and fMRI data from BASELINE, NAUSEA, and RECOVERY 4-min windows. A percept-based analysis evaluated autonomic and fMRI data from the 0 to 1, 1 to 2, and 2 to 3 nausea rating transitions, where data from 30 s before the transition were compared with data from 30 s after the transition.

Data Preprocessing

Heart Rate and Heart Rate Variability

R–R intervals were obtained annotating ECG data (16 nausea prones and 8 controls) through automated methods (WaveForm DataBase Software Package, PhysioNet, MIT) followed by manual adjustments, in order to assure correct peak detection. Following ECG R-wave beat annotation, we applied a point process method used to develop local likelihood (Barbieri et al. 2005) HR estimation. This was applied to the R–R series, in order to compute instantaneous estimates of HR and HRV. The stochastic structure assumed to generate the R-wave events is modeled as a history-dependent inverse Gaussian process, as its explicit probability density is derived directly from an elementary, physiologically based integrate-and-fire model (Barbieri et al. 2005). Modeling the mean of the R–R interval lengths as a linear function of the last k R–R intervals allows us to subsequently estimate the dependence of such intervals on the recent history of parasympathetic and sympathetic inputs to the sinoatrial (SA) node of the heart. The estimation of the total spectral power and further extraction of the high-frequency (HF, 0.15–0.5 Hz) spectral component was derived from this estimated set of k regressive coefficients. By exploiting this approach, the dynamics of the model parameters, and consequently the time-varying behavior of the spectral indices, could be estimated at any time resolution. This was critical in estimating the temporal dynamics with a resolution matched to the temporal resolution of the fMRI signal.

In this work, we considered the instantaneous HR index computed from the point process model as our measure of HR, and the instantaneous HF-HRV index as our representative metric for parasympathetic activity. The HR and HF-HRV series were estimated using a fixed model order $k = 8$, every $\Delta = 2$ ms, low-pass filtered at 0.33 Hz, and resampled at the fMRI TR time points. Before being used as regressors in the fMRI analysis, the HF-HRV power was thresholded under the 98th percentile. This process was necessary in order to enhance sensitivity to the full-range dynamics of the HF-HRV time series, and not a limited number of outlier time series values, when used in conjunction with the fMRI general linear model (GLM) analysis (see below).

Skin Conductance Level

Skin conductance level is a known marker of sympathetic outflow to the sudomotor glands of the skin (Gray et al. 2009). The signals (11 nausea prone and 5 controls) were low-pass-filtered at 0.33 Hz and resampled at the fMRI sampling frequency, in order to be used in the fMRI GLM analysis.

Functional MRI

The preprocessing of BOLD data was performed using FSL (v5.0, FMRIB's Software Library) and included field map correction, brain extraction, motion correction, high-pass filtering ($f > 0.007$ Hz), spatial smoothing (FWHM = 5 mm), and spatial normalization to Montreal Neurological Institute (MNI) space.

Data Analysis

Our analysis of the central autonomic response to nausea used both a stimulus-based approach and a percept-based approach, allowing for different methodological approaches in combining ANS outflow data with synchronized fMRI data. For the stimulus-based approach, both peripheral autonomic and brain BOLD data were first analyzed within 3 different temporal windows: Specifically, the 4-min window prior to the onset of the visual nauseogenic stimulation (henceforth "BASELINE," B), the last 4-min window before the visual nauseogenic stimulation terminated ("NAUSEA," N), which comprised the most severe nausea experienced, and the first 4-min window of the second visual fixation period ("RECOVERY," R), in order to examine the recovery process after the nauseogenic stimulus had terminated (Fig. 1). Note that for non-nausea-prone control subjects, the NAUSEA and RECOVERY windows were not associated with significant nausea sensation. The duration of the time window (4 min) was chosen to balance potential nonstationarity within the window with the need for adequate data vector size for both HRV and BOLD data analyses (LaCount et al. 2011).

Mean HR, HF-HRV, and SCL values were calculated across subjects for each time window, and NAUSEA and RECOVERY values were

compared with BASELINE using a Student's paired *t*-test. Bonferroni correction was adopted to correct for multiple comparisons, and significance was set at $P = 0.05$.

In order to obtain the brain correlates of autonomic modulation related to nausea, BOLD data were similarly split into 4-min datasets relative to each time window (BASELINE, NAUSEA, and RECOVERY) and analyzed using HF-HRV and SCL regressors. These regressors were formed by convolving the ANS signal time series with a canonical gamma hemodynamic response function (HRF, SD = 3 s, mean lag = 6 s). Separate subject-level GLMs for each time window were evaluated for these regressors. We should note that HR was not adopted as a regressor of interest in this analysis given its lack of specificity as an autonomic metric (i.e. HR is influenced by both sympathetic and parasympathetic efference). Instead, the HR time series was used to control for cardiogenic (non-neural) artifact in the brain. The HR time series was resampled at the fMRI TR and convolved with a specific cardiac response function (Chang et al. 2009) known to reflect this pulsatile artifact. This confound regressor was added to the GLM, and statistical parametric mapping was carried out using the FMRI Expert Analysis Tool (FEAT v.5.90, FSL).

Parameter estimates derived from each subject were then passed up, with their variances, to group-level mixed-effects analyses (FLAME, FEAT, FSL) (Beckmann et al. 2003). Group maps for each time window (BASELINE, NAUSEA, and RECOVERY) were calculated for both HF-HRV and SCL regressors, as an estimate of the central autonomic activity related to cardiovagal and skin sudomotor (sympathetic) modulation. We also evaluated difference maps for central autonomic network activity contrasting (1) NAUSEA and (2) RECOVERY with respect to BASELINE, using paired *t*-tests.

In order to more closely link autonomic changes with changes in autonomic-associated brain response, individual HF-HRV and SCL difference scores between time windows were used as a regressor of interest in group-level regression analyses with HF-HRV and SCL-based fMRI difference maps (see above) as dependent variable. In this case, given the high asymmetry of HF-HRV power variations across subjects, individual changes were normalized with respect to BASELINE values, thus obtaining relative, normally distributed (Lilliefors test, $P = 0.27$) variations. This procedure allowed us to disentangle the change in HF-HRV power from the initial baseline value as these measures were highly correlated (Spearman's rho = −0.93, $P < 0.001$). As an aside, the same normalization procedure was not necessary for SCL values (Lilliefors test on absolute data, $P > 0.5$). Hence, in order to identify whether any of the brain regions from the difference map analyses reported above also showed a correlation with the mean variations between time windows for HF-HRV and SCL, the correlation analysis maps were masked with the results of the difference analysis maps after thresholding.

In addition to the stimulus-based analysis described earlier, a percept-based approach further explored the neural correlates of autonomic outflow relative to nausea-prone subjects' individual nausea ratings. FMRI data from nausea-prone subjects were split into 1-min datasets, temporally centered on each nausea transition reported by subjects—that is, change from lower to higher nausea (30 s before and 30 s after rating change, Fig. 1). Only "0 to 1," "1 to 2," and "2 to 3" transitions were included, since transition to level "4" coincided with the termination of the visual stimulus, thus introducing a brain response not related to nausea increase. For our percept-based analysis, we used HR and SCL time series from these 1-min windows, as these measures were the only ones responsive to ratings of nausea increase (see below). HR or SCL change scores for each transition were used as independent variable and tonic brain response [post- versus pre-rating change, similar to that used in our previous publication (Napadow et al. 2013)] was used as dependent variable in a group-level linear regression analysis.

All resultant statistical brain maps noted above were corrected for multiple comparisons and family-wise error with a cluster forming threshold of Z = 2.3 and cluster corrected at $P < 0.05$.

In Figure 2, the whole analysis pathway is shown, starting from parallel analyses of ANS and fMRI data, and then integrated through combined GLM analyses for both the stimulus-based approach and the percept-based approach. References to the figures and tables reporting the results from each step are also included in this diagram.

Results

Behavioral and Autonomic Data Analysis

Eleven of the 17 nausea-prone subjects completing the MRI scan session reported a rating of "4," indicating "severe" nausea with the urge to vomit, thus terminating the stimulus before the maximum 20 min. The other 6 nausea-prone subjects rated at least moderate nausea (2 of 4) during the last 4 min of the stimulus. For the non-nausea-prone control subjects, 6 of 8 did not rate any nausea sensation during the duration of the experiment, whereas the remaining 2 subjects reported a mild nausea sensation (1 of 4) during the visual stripes stimulation.

For the stimulus-based analysis, autonomic indices were compared between (1) the NAUSEA and (2) RECOVERY 4-min temporal windows and BASELINE for both nausea-prone and control subjects (Fig. 3). Significant differences between nausea-prone subjects and healthy controls were confirmed through a 2 × 2 ANOVA (group × condition) for each autonomic index (HR: $F_{(1,1)} = 14.83$, $P = 0.0004$; HF-HRV: $F_{(1,1)} = 4.65$, $P = 0.0365$; SCL: $F_{(1,1)} = 15.55$, $P = 0.0005$). For nausea-prone subjects, HR increased significantly compared with BASELINE during NAUSEA ($\Delta = 12.3 \pm 1.8$ beats per minute (bpm), mean ± SEM, $P < 0.001$) and RECOVERY ($\Delta = 5.8 \pm 2.1$ bpm, $P < 0.05$). No significant changes in HR were found for non-nausea-prone control subjects (NAUSEA–BASELINE: $\Delta = 0.6 \pm 0.9$ bpm; RECOVERY–BASELINE: $\Delta = 1.1 \pm 1.0$ bpm), who did not report significant nausea during the experiment.

With regard to HF-HRV power, nausea-prone subjects demonstrated a significant decrease during the last 4 min of nauseogenic stimulus with respect to BASELINE ($\Delta = -1672.2 \pm 657.4$ ms^2, $P < 0.05$), whereas the change for RECOVERY–BASELINE did not reach significance ($\Delta = -832.8 \pm 455.6$ ms^2, $P = 0.17$). No significant changes in HF-HRV were found for non-nausea-prone control subjects (NAUSEA–BASELINE: $\Delta = 79.7 \pm 315.2$ ms^2; RECOVERY–BASELINE: $\Delta = -65.5 \pm 193.8$ ms^2, Fig. 3A).

For nausea-prone subjects, SCL also increased significantly from BASELINE for both the NAUSEA ($\Delta = 2.0 \pm 0.4$ µS, $P < 0.05$) and RECOVERY ($\Delta = 2.53 \pm 0.4$ µS, $P < 0.001$) temporal windows. No significant changes in SCL were found for non-nausea-prone control subjects (NAUSEA–BASELINE: $\Delta = 0.2 \pm 0.4$ µS; RECOVERY–BASELINE: $\Delta = 0.5 \pm 0.4$ µS) (Fig. 3A).

For nausea-prone subjects, the change scores comparing RECOVERY versus NAUSEA were significant for all 3 autonomic metrics (HR: $\Delta = -6.5 \pm 1.1$ bpm, $P < 0.001$; SCL: $\Delta = 0.5 \pm 0.2$ µS, $P < 0.05$; HF-HRV: $\Delta = 839.4 \pm 268.9$ ms^2, $P < 0.05$; Fig. 3A). Thus, HR decreased, whereas HF-HRV and SCL increased during RECOVERY compared with NAUSEA.

We also evaluated potential cross-correlation between HF-HRV changes and SCL changes. We did not find any significant cross-correlation between autonomic metrics within specific temporal window contrasts (NAUSEA–BASELINE: Spearman's rho = −0.25; RECOVERY–BASELINE: Spearman's rho = −0.27) nor between metrics across different temporal windows (NAUSEA–BASELINE [HF-HRV] versus RECOVERY–BASELINE [SCL]: Spearman's rho = −0.13). Thus, subjects with greater HF-HRV change did not also demonstrate greater SCL change, nor did subjects with greater HF-HRV change during NAUSEA also demonstrate greater SCL change during RECOVERY.

For the percept-based analysis, SCL increased significantly for all increasing nausea rating transitions, with the greatest change for the "0 to 1" rating transition ("0 to 1": $\Delta = 0.83 \pm 0.33$ µS, $P <$

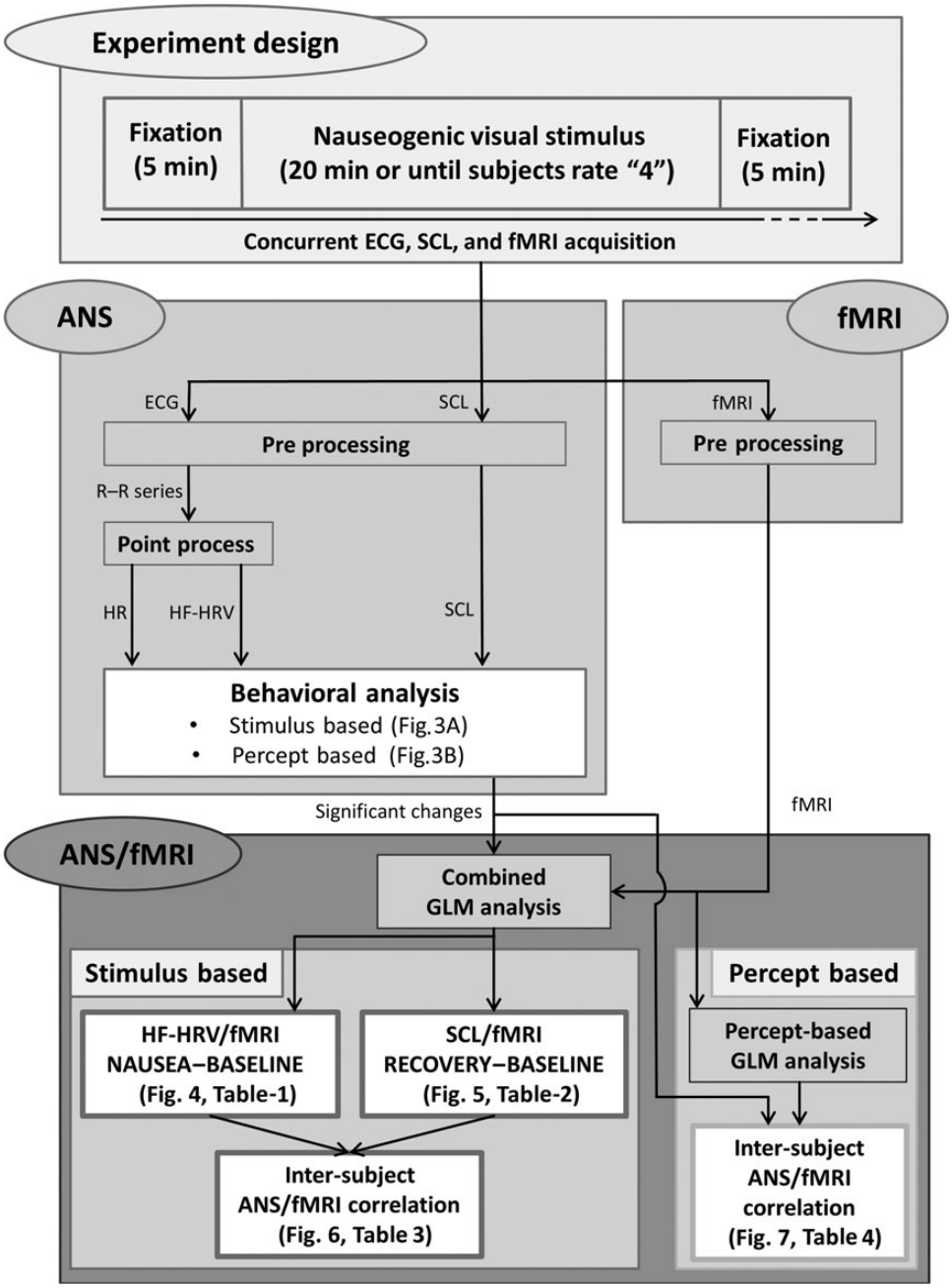

Figure 2. Schematic diagram of the analysis pipeline. ANS and fMRI data concurrently acquired during the nauseogenic stimulation are first preprocessed separately. Significant changes highlighted by the behavioral data analysis are then combined with fMRI data through GLM analyses, both for the stimulus-based approach and for the percept-based approach. The outcomes of each analysis step are also reported in the related sub-blocks.

0.05; "1 to 2": $\Delta = 0.51 \pm 0.19$ μS, $P < 0.05$; "2 to 3": $\Delta = 0.38 \pm 0.13$ μS, $P < 0.001$) (Fig. 3B). HR showed acceleration in response to rating increases, but only the "1 to 2" transition was significant ("0 to 1": $\Delta = 3.19 \pm 1.78$ bpm; "1 to 2": $\Delta = 4.17 \pm 1.39$ bpm, $P < 0.001$; "2 to 3": $\Delta = 2.29 \pm 1.75$ bpm) (Fig. 3B). Finally, HF-HRV changes were not significant for any of the rating increases ("0 to 1": $\Delta = 68.7 \pm 331.8$ ms^2; "1 to 2": $\Delta = -313.9 \pm 122.8$ ms^2; "2 to 3": $\Delta = -173.4 \pm 200.6$ ms^2) (Fig. 3B).

Combined Autonomic–fMRI Analyses

The central autonomic network response to nausea was estimated by using autonomic outflow metrics to guide the fMRI data analysis. For the stimulus-based analysis, we used the HF-HRV and SCL signals, convolved with the HRF, as regressors in the GLM. The stimulus-based paired difference maps reflected differential activity for NAUSEA–BASELINE and RECOVERY–BASELINE windows. As HF-HRV and SCL signals were significantly changed from BASELINE for nausea-prone (NAUSEA window for HF-HRV, and both the NAUSEA and RECOVERY windows for SCL) but not control subjects, this analysis was focused on nausea-prone subjects for windows showing significant ANS change only. The 2 differential maps reported in Figure 4 and Figure 5 resulted from paired *t*-tests between time windows. In order to show which of the

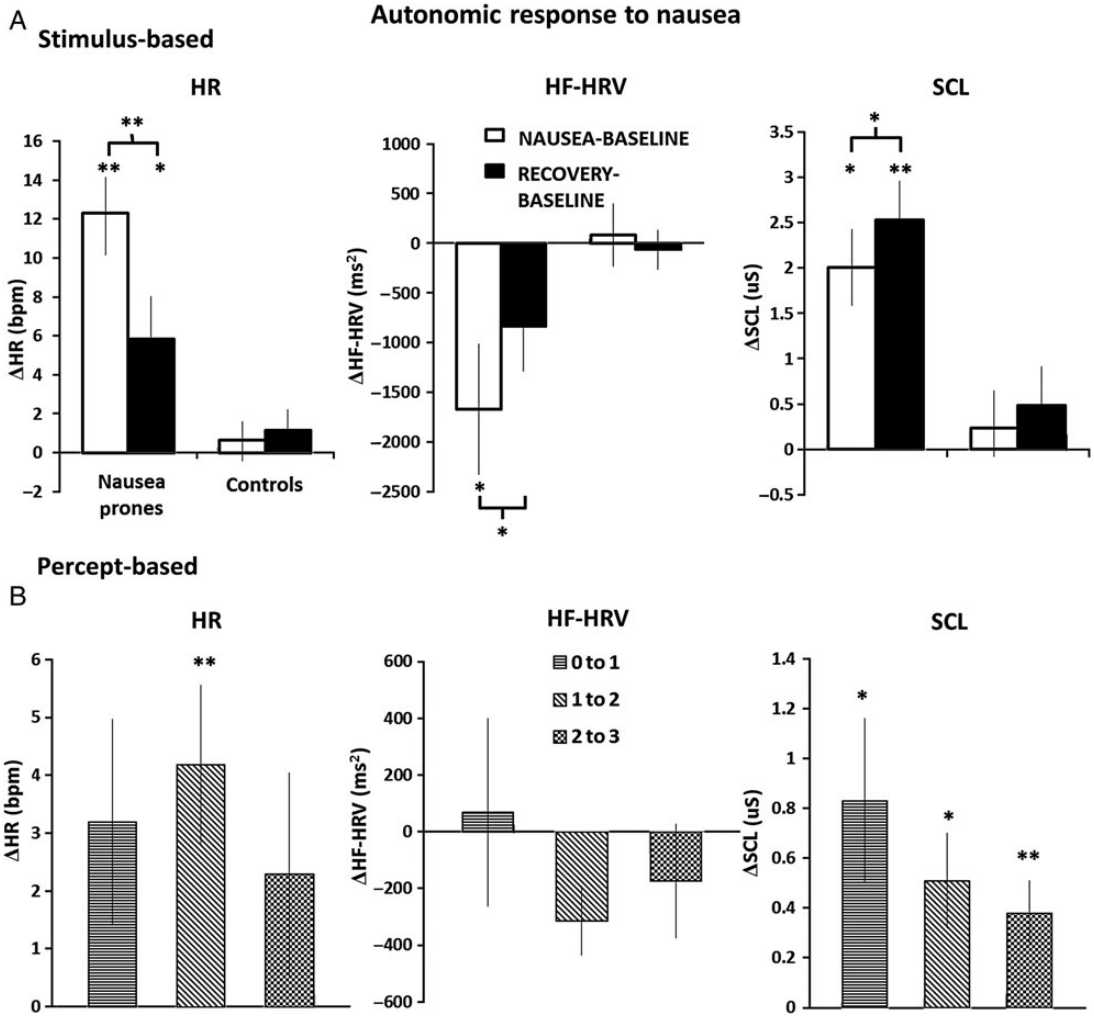

Figure 3. (*A*) Autonomic response to nausea for the stimulus-based analysis: HR, HF-HRV, and SCL variations (mean ± SEM) with respect to BASELINE for both nausea-prone and control subjects. (*B*) Autonomic response to nausea for the percept-based analysis: HR, HF-HRV, and SCL transitions to higher nausea states (mean ± SEM). Note: $^{*}P < 0.05$; $^{**}P < 0.001$; statistical significance testing was Bonferroni-corrected for multiple comparisons.

2 conditions (e.g. BASELINE or NAUSEA–RECOVERY) was driving the significant difference reported, bar plots reported mean signal intensity response associated with different ANS regressors extracted from BASELINE, NAUSEA, or RECOVERY maps, respectively, from the peak voxel of brain regions identified in the paired *t*-test difference map.

Compared with BASELINE, we found that NAUSEA produced an increased negative relationship between HF-HRV and fMRI signals in a diffuse network of brain regions including medial prefrontal cortices (mPFC)/anterior mid-cingulate cortices (aMCC) and posterior cingulate cortices (PCC), ventral middle/posterior (vm/pIns) and posterior (pIns) insulae, para-hippocampus (PHG), supramarginal gyrus (SMG), and superior temporal gyrus, and lateral temporal cortex (LTC). Other regions showing this pattern included fusiform gyrus (FuG), inferior parietal lobule (angular gyrus, AnG), primary and secondary somatosensory (S1, S2), premotor and motor (preMC, M1), and primary visual (V1) and extrastriate cortices consistent with MT+/V5, as well as cerebellum (lobules V, VI, VIIIB, IX) (Fig. 4, Table 1).

Compared with BASELINE, we found that RECOVERY produced an increased negative relationship between SCL and fMRI signals in the dorsomedial (dmPFC), ventrolateral (vlPFC), and dorsolateral (dlPFC) prefrontal and orbitofrontal (OFC) cortices, dorsal and ventral anterior insula (daIns, vaIns), inferior (AnG) and superior (SPL) parietal lobules, and precuneus (PCun) (Fig. 5, Table 2). There were no significant differences in SCL-associated central autonomic network activity for the NAUSEA versus BASELINE differential window analysis.

In addition to the difference map analyses reported earlier, a closer linkage between peripheral autonomic outflow and brain activity was evaluated by correlating individual differences of ANS–fMRI parameter estimates with matching variations in autonomic responses. Difference maps for both HF-HRV and SCL/fMRI analyses showed negative correlation with the mean change in autonomic indices within brain regions previously identified by the original differential analysis. For the HF-HRV correlation analysis, all of the brain areas noted in Table 1 (with the exclusion of PCC) demonstrated a significant correlation with the change in HF-HRV between the NAUSEA and BASELINE windows (Fig. 6, Table 3). For the SCL correlational analysis, left dlPFC (middle frontal gyrus) and vlPFC demonstrated a significant correlation with the change in SCL between the RECOVERY and BASELINE windows (Fig. 6, Table 3).

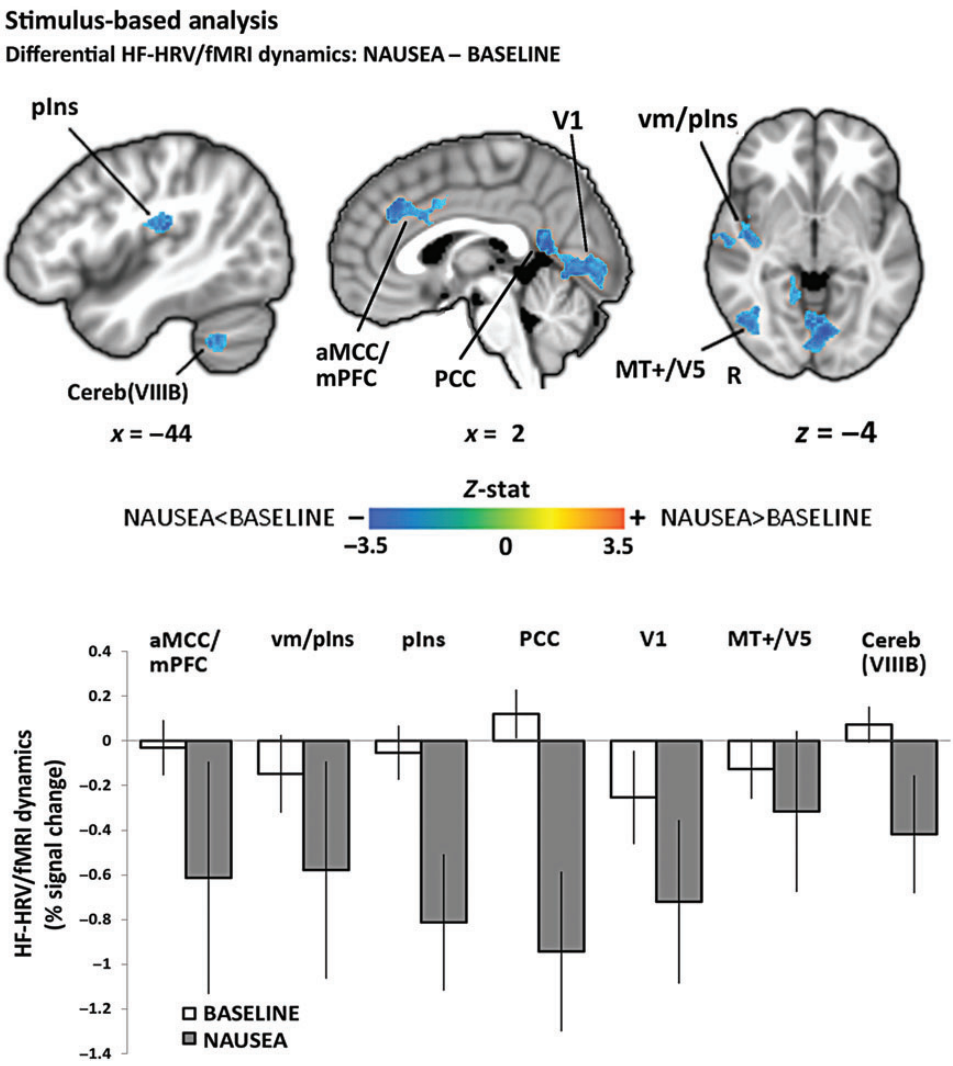

Figure 4. Stimulus-based HF-HRV/fMRI analysis: NAUSEA–BASELINE differential response included brain regions such as mPFC/aMCC and PCC, middle insula, primary visual areas, and extrastriate cortices, as well as cerebellum. An increased negative relationship during NAUSEA with respect to BASELINE was found in all the involved areas. Bar plot error bars represent standard error of the mean (SEM).

For the percept-based analysis, a group-level regression was performed between the change in autonomic index post- minus pre-nausea rating change versus the change in brain activity associated with this transition for nausea-prone subjects. We found a negative correlation for both HR and SCL indices. Specifically, greater increase in both HR and SCL (Fig. 7, Table 4) was associated with greater deactivation in right and left mid-insular cortex, respectively. Other brain regions showing greater deactivation were left IPL, bilateral temporal gyrus, and MT+/V5 for greater HR increases, and cerebellum for greater SCL increases. There were no significant correlations for HF-HRV post- minus pre-nausea rating change, consistent with behavioral data results, which showed no significant changes in HF-HRV for any rating change period (Fig. 3B).

Discussion

The central autonomic network supporting nausea-induced sympathetic and parasympathetic outflow was evaluated, and our results demonstrated that brain regions such as the insula were strongly associated with both sympathetic and parasympathetic outflow. Results from behavioral analysis confirmed the strong autonomic response to the nauseogenic stimulus, showing an increase in sympathetic outflow and a concurrent decrease in parasympathetic outflow. Interestingly, activity in default mode network regions and brain regions processing visual motion were most strongly associated with parasympathetic outflow, which was maximally decreased at peak nausea perception. In contrast, brain regions such as the lateral prefrontal cortex were most strongly associated with sympathetic outflow, which was maximally increased after cessation of the nauseogenic stimulation, when subjects were still nauseous but in recovery.

The brain regions supporting sympathetic versus parasympathetic response differed substantially, supporting a divergence in central control over the 2 ANS divisions. Such divergence has also been noted for other ANS-modulating stimuli by a prior neuroimaging meta-analysis (Beissner et al. 2013). In fact, the only regions involved in both sympathetic

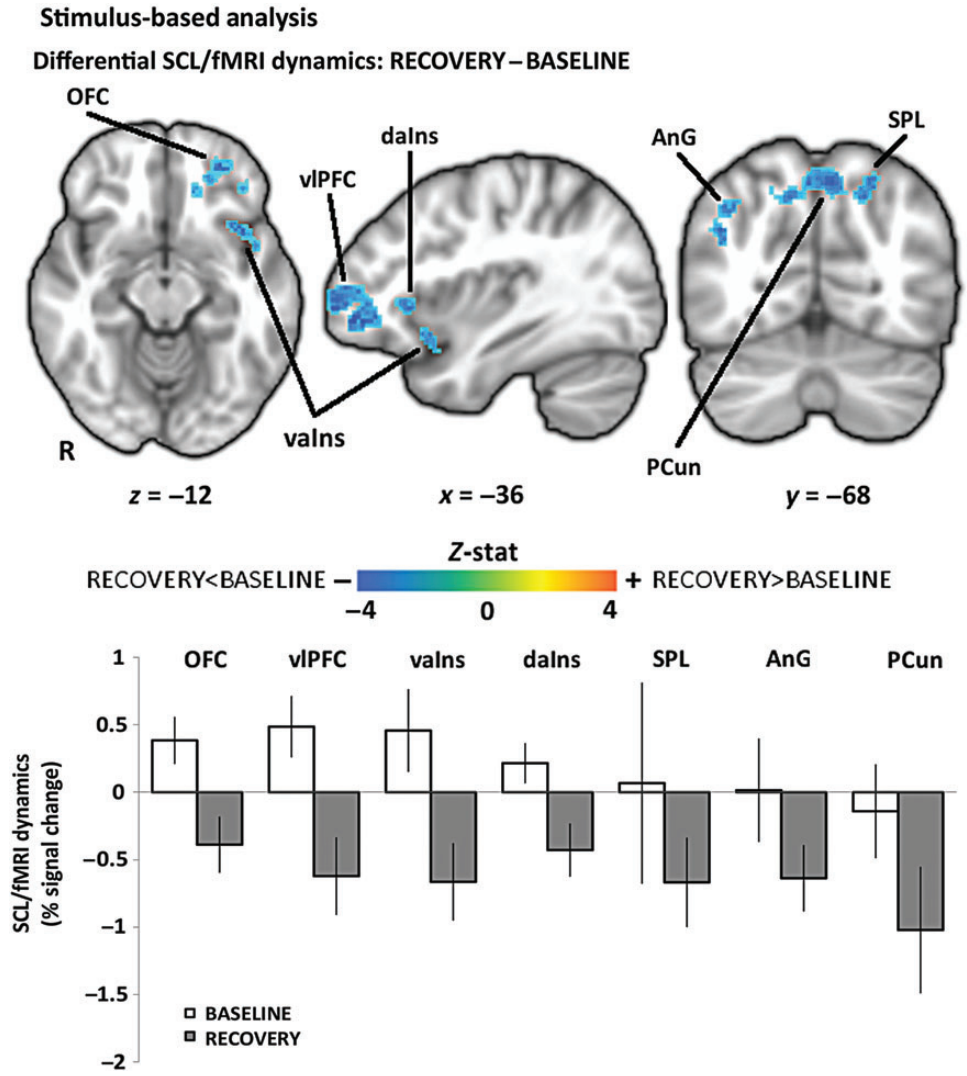

Figure 5. Stimulus-based SCL/fMRI analysis: RECOVERY–BASELINE differential response included brain regions such as vlPFC prefrontal and orbitofrontal cortices, anterior insula, inferior and superior parietal lobule, and precuneus. An increased negative relationship during RECOVERY with respect to BASELINE was found in all the involved areas. Bar plot error bars represent SEM.

and parasympathetic modulation were the insula and inferior parietal lobule, regions also implicated as having more generalized function by this previous meta-analysis. Interestingly, while mid/posterior insula was implicated in parasympathetic processing, anterior/mid insula was implicated in sympathetic processing. This posterior shift of insular subregions in processing different divisions of the ANS appears to also be consistent with sympathetic/parasympathetic differentiation in previous ANS–fMRI studies (Beissner et al. 2013). In addition to ANS division specialization, insula subregion involvement may also relate to organ specificity (i.e. skin versus heart) as well as differential temporal response properties. In general, autonomic processing via insula activity is consistent with the insula's oft-mentioned role in interoception (Craig 2002; Critchley et al. 2004; Wiens 2005), defined as conscious awareness of internal body states (Craig 2002), as interoceptive afference is commonly carried by general visceral afferent (autonomic) fibers. Since insular (anterior, middle, and posterior) along with mid-cingulate cortex activation was also found in response to nausea (Napadow et al. 2012), our results demonstrate that these interoception processing brain regions (Mayer et al. 2009) also play a critical role in autonomic modulation by nausea.

Importantly, for both the HF-HRV and SCL analyses, an increased negative correlation between ANS metric and fMRI signal was found during the NAUSEA and RECOVERY time windows relative to BASELINE, respectively. This suggests that many of the regions implicated by our analysis had inhibitory influence on premotor autonomic nuclei in the medulla and that this inhibitory influence was magnified during periods of nausea perception, when autonomic outflow was significantly modulated. Hence, this altered brain response linked to autonomic outflow may serve as a coping mechanism in nausea-prone subjects, trying to limit the magnitude of efferent autonomic response and ultimately nausea sensation in response to the visual stimulus. Despite early studies questioning ANS activity as a marker for nausea (Money 1970), multiple lines of evidence support the importance of autonomic activity in the generation and perception of nausea (see review, Muth 2006). Our own human research found that "dynamic HF-HRV. .

Table 1
Stimulus-based HF-HRV/fMRI analysis: NAUSEA–BASELINE-associated brain regions

Brain region	Side	Location (MNI)			*Z*-score
		x	*y*	*z*	
aMCC/mPFC	R	2	32	36	−3.31
vm/pIns	R	44	2	−10	−3.05
pIns	L	−42	−26	20	−3.27
M1	L	−56	−8	48	−2.99
preMC	L	−57	16	26	−3.25
S1	L	−58	−10	40	−3.05
S2	L	−64	−20	16	−2.99
PCC	L	−2	−54	14	−3.84
AnG	L	−62	−32	36	−3.21
SMG	L	−60	−18	36	−3.5
LTC	R	58	−20	4	−3.37
—	L	−54	−20	8	−3.34
PHG	L	−34	−32	−20	−3.05
V1	R	6	−78	4	−3.09
—	L	−4	−80	2	−3.01
MT + /V5	R	42	−78	16	−3.24
FuG	R	38	−56	−10	−3.26
Cereb(V)	R	16	−46	−22	−3.13
Cereb(VI)	L	−38	−42	−32	−3.29
Cereb(VIIIB)	L	−26	−42	−40	−3.33
Cereb(IX)	R	14	−56	−40	−3.21

Table 2
Stimulus-based SCL/fMRI analysis: RECOVERY–BASELINE-associated brain regions

Brain region	Side	Location (MNI)			*Z*-score
		x	*y*	*z*	
OFC	L	−28	48	−12	−3.6
vlPFC	L	−42	48	−4	−4.08
dmPFC	L	−6	56	10	−3.01
dlPFC	L	−46	38	24	−3.23
vaIns	L	−38	16	−12	−3.53
daIns	L	−36	24	0	−3.31
SPL	L	−20	−70	48	−3.56
AnG	R	42	−68	30	−3.31
PCun	R	4	−66	50	−3.7
—	L	−6	−68	50	−3.4

. bursts of cardiovagal modulation precede rating transitions to higher nausea" (LaCount et al. 2011), allowing for a potential causal effect. Interestingly, Stern (2002) suggested a model by which motion sickness produces autonomic outflow, which induces gastric tachyarrhythmia and feeds back to the brain to produce nausea perception. Such feedback may be interpreted in the context of the James–Lange theory of emotion (Lang 1994), which suggests a causal linkage between autonomic/humoral outflow (higher adrenaline level, heartbeat, etc.) and affective response to arousal stimuli, though such connections are likely more complex than a simple one-way causal link. In sum, while cardiac and sudomotor activity may or may not be part of a causal chain of events leading up to the conscious perception of nausea, ANS outflow is at least an important and robust marker, and a better understanding of the underlying brain activity may aid in understanding individual variability in both conscious nausea perception and heterogeneity in ANS response to that perception.

Negative correlation was found for both the stimulus-based analysis between m/pIns signal and HF-HRV power during NAUSEA, and the percept-based analysis between mIns signal and both HR and SCL response for transitions to higher levels of nausea. Interestingly, for the stimulus-based analysis, greater HF-HRV decrease with respect to BASELINE was associated with reduced anti-correlation between fMRI signal in m/pIns and HF-HRV power (i.e. parasympathetic modulation). This might be explained by the fact that reduced HF-HRV power leads to reduced signal dynamics and ultimately reduced correlation to mIns fMRI signal. In contrast, for the percept-based analysis, greater HR or SCL increase to increasing nausea (i.e. increased sympathetic outflow) was associated with greater mIns deactivation, consistent with a direct inhibitory role of mIns activity on sympathetic premotor activity in the brainstem.

Pooled together, many of the brain regions supporting ANS response to nausea are consistent with those proposed as key regulatory areas of autonomic outflow in recent reviews and meta-analyses concerning the central autonomic network (Beissner et al. 2013; Shoemaker et al. 2012; Thayer et al. 2012). These regions include cingulate, insular, prefrontal, and orbitofrontal cortices. Conversely, many subcortical and brainstem areas associated with central autonomic control, such as amygdala, thalamus, hippocampus, and brainstem nuclei (Macefield et al. 2013; Jänig 2006; Saper 2002), were not identified by our analysis. Physiological artifacts from cardiorespiratory sources hamper neuroimaging in brainstem regions, requiring a more focused approach (Brooks et al. 2013), which in our case is especially acute as there is a need to account for non-neuronal cardiorespiratory pulsatile artifact without sacrificing signal variance attributable to neural activity associated with cardiorespiratory (i.e. autonomic) outflow.

In our stimulus-based analysis, parasympathetic-associated brain activity was found to be much more widespread than sympathetic-associated activity and included brain areas not typically associated with autonomic regulation. These areas included visual processing regions such as V1 and MT + /V5. This was probably due to an interaction between brain response to the nauseogenic visual stimulation during NAUSEA and dynamics in parasympathetic outflow. In contrast, during the RECOVERY time window, when sympathetic outflow was most increased, visual stimulation was confined to simple crosshair fixation and produced less robust primary visual and extrastriate activation. Interestingly, a recent study has implicated many of the regions identified by our parasympathetic-fMRI analysis during NAUSEA as areas coding specific parameters of visually induced self-motion (Becker-Bense et al. 2012). Specifically, cerebellar vermis and parieto-occipital regions showed significantly enhanced activation during circular vection, whereas parietal areas (IPL, bilateral PCun) were found to process the intensity of perceived vection, attributable to the dorsal stream ("where or how" pathway), which is mediated by information transfer from primary visual areas to the parietal lobe (de Haan and Cowey 2011). Moreover, Lobel et al. (1998) found that vection induced by galvanic (i.e. nonvisual) stimuli produces activation in superior and inferior posterior parietal cortex, whereas we found ANS-BOLD correlations in the left AnG and SMG for parasympathetic-related structures and in the left SPL for sympathetic-related structures. In sum, in our study, greater visual and self-body motion processing due to the nauseogenic stimulus likely led to higher activity in these visual and vection processing areas and was associated with altered parasympathetic or sympathetic modulation. Hence, while visual processing areas such as V1 and MT + /V5 and vection processing areas in the posterior parietal lobule are likely not directly linked with premotor autonomic nuclei in the medulla, ANS

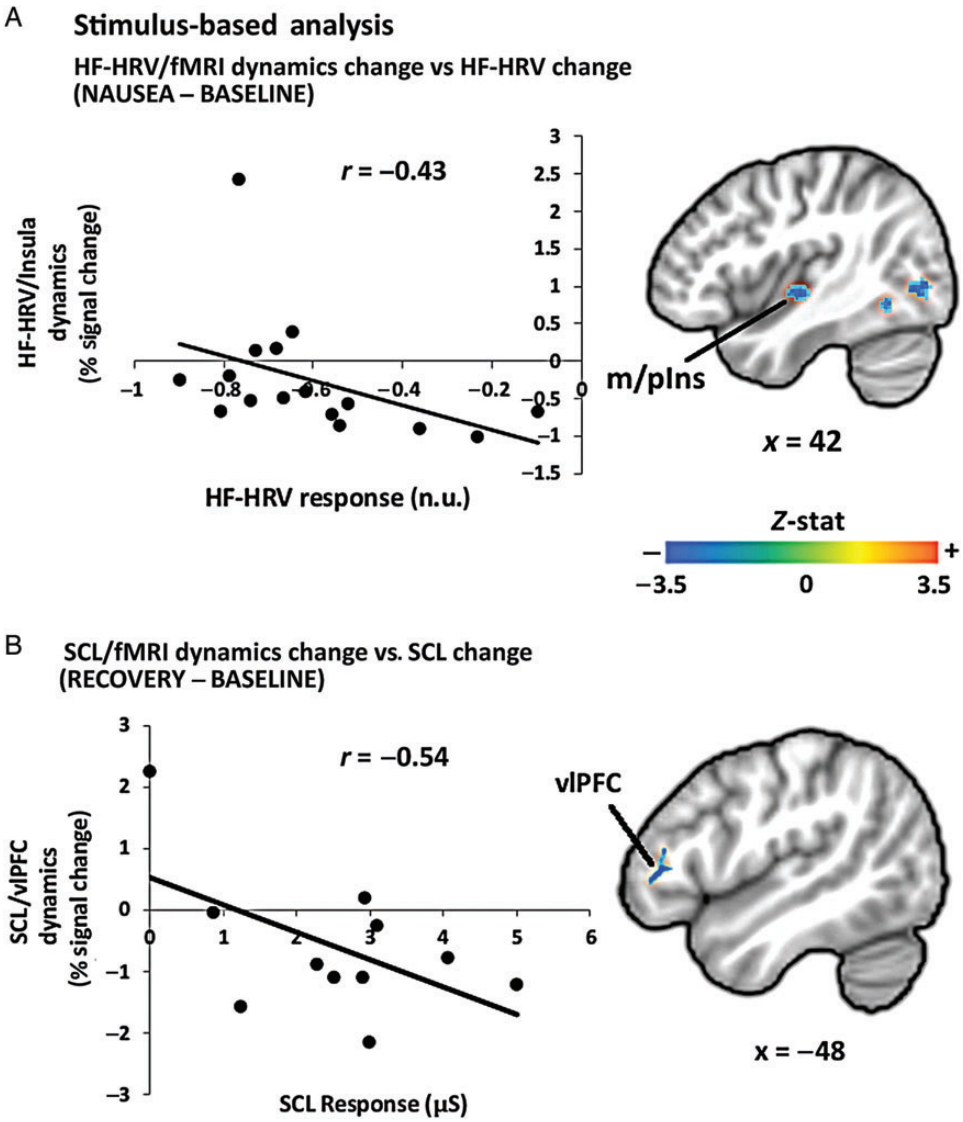

Figure 6. Stimulus-based analysis: inter-individual correlation between (A) change in HF-HRV/fMRI insular cortex response and change in HF-HRV (NAUSEA–BASELINE); (B) change in SCL/fMRI vlPFC prefrontal cortex response and change in SCL (RECOVERY–BASELINE. Note: r = Pearson's correlation coefficient; r^* = –0.63, Pearson's correlation coefficient removing the outlier (–0.77; 2.43), as determined by Grubb's test for outliers.

outflow due to nauseogenic visual stimulation likely involves information transfer from these brain areas to areas more intimately linked with ANS outflow, such as the insula.

Consistent with our previous study (LaCount et al. 2011), the stimulus-based analysis showed increased HR and skin conductance, as well as decreased HF-HRV, during a 4-min window when nausea was most intense. Previous studies have noted a heterogeneous HF-HRV response to nausea (Doweck et al. 1997; Kim et al. 2005; LaCount et al. 2011; Mullen et al. 1998; Yokota et al. 2005), and Lin et al. recently suggested that this heterogeneity may be due to variability in nausea-induced changes in respiratory rate and/or volume between studies (Lin et al. 2011, 2013). In our study, subjects were asked to maintain constant respiration, which likely limited the influence of respiratory changes on HF-HRV response to nausea. In fact, our previous study did not find any significant change in respiratory rate for similar duration windows (LaCount et al. 2011). Interestingly, our percept-based SCL analysis showed the greatest sympathetic increase following the 0–1 nausea transition, consistent with McClure et al. (1971), which found that skin conductance, measured from the palmar aspect of the hand, may be a marker of early arousal during motion sickness. However, as reported by our previous study (LaCount et al. 2011) and as shown in Figure 1 for a representative subject and confirmed by the analysis of tonic SCL group data (Fig. 3A), the activity recorded on the palmar aspect of the finger tips clearly increases, gradually, as the visual stimulus continues and increasing nausea sensations are reported by the subjects. Moreover, all transition to higher nausea levels (including 1-to-2 and 2-to-3 transitions) also resulted in phasic increases following transitions (Fig. 3B), supporting the idea that SCL increase accompanies both phasic transitions and gradually increasing nausea sensation.

Another interesting finding was that the greatest changes in HF-HRV and SCL were found for the final 4 min of nauseogenic stimulation (NAUSEA–BASELINE) and for the 4 min after

Table 3
Stimulus-based analysis: inter-individual correlation between change in ANS/fMRI association and change in ANS response

Brain region	Side	Location (MNI)			*Z*-score
		x	*y*	*z*	
HF-HRV					
aMCC/mPFC	L	−2	32	34	−2.99
m/pIns	R	44	−12	−4	−3.16
pIns	L	−42	−24	16	−2.49
M1	L	−56	−8	50	−3.09
preMC	L	−54	10	26	−3.01
S1	L	−58	−10	40	−3.05
S2	L	−64	−20	16	−2.99
AnG	L	−62	−32	36	−3.21
SMG	L	−60	−18	36	−3.5
LTC	R	58	−20	4	−3.37
—	L	−54	−20	8	−3.34
PHG	L	−34	−32	−20	−3.05
V1	L	−6	−72	−2	−3.61
—	R	6	−70	−2	−3.39
MT + /V5	R	42	−70	−2	−3.09
FuG	R	38	−56	−10	−3.26
Cereb(V)	R	16	−46	−22	−3.13
Cereb(VI)	L	−38	−46	−32	−2.77
Cereb(VIIIB)	L	−26	−46	−40	−3.13
Cereb(IX)	R	14	−56	−40	−3.21
SCL					
vlPFC	L	−48	36	10	−3.12
dlPFC	L	−56	14	28	−2.58

removal of this stimulus (RECOVERY–BASELINE), respectively. A similar result was also found in our previous study (LaCount et al. 2011), where the instantaneous estimate of HF-HRV was found to increase back toward baseline values within tens of seconds after cessation of the nauseogenic stimulus, whereas SCL showed persistent elevated values into this post-stimulus recovery period. The persistence of sympathetic activation into the recovery period is likely a manifestation of the known long latency characterizing this division of the ANS (Boucsein 2012). Also, the work by Sheehan et al. (2011) noted the difficulty of clearly attributing motion sickness to the unique modulation of either sympathetic ("fight or flight") or parasympathetic ("rest and relax") autonomic responses, thus supporting our results showing the absence of coordination between the 2 ANS branches. For instance, we found greater increase in sympathetic activity after the cessation of the visual stimulus, whereas parasympathetic (cardiovagal) activity decreased most significantly during peak nausea and rapidly returned toward baseline values after stimulus cessation. Moreover, our results did not find significant correlation between HF-HRV and SCL changes. That is, subjects with greater HF-HRV change did not also demonstrate greater SCL change during the same time window (i.e. NAUSEA or RECOVERY), nor did subjects with greater HF-HRV change during NAUSEA also demonstrate greater SCL change

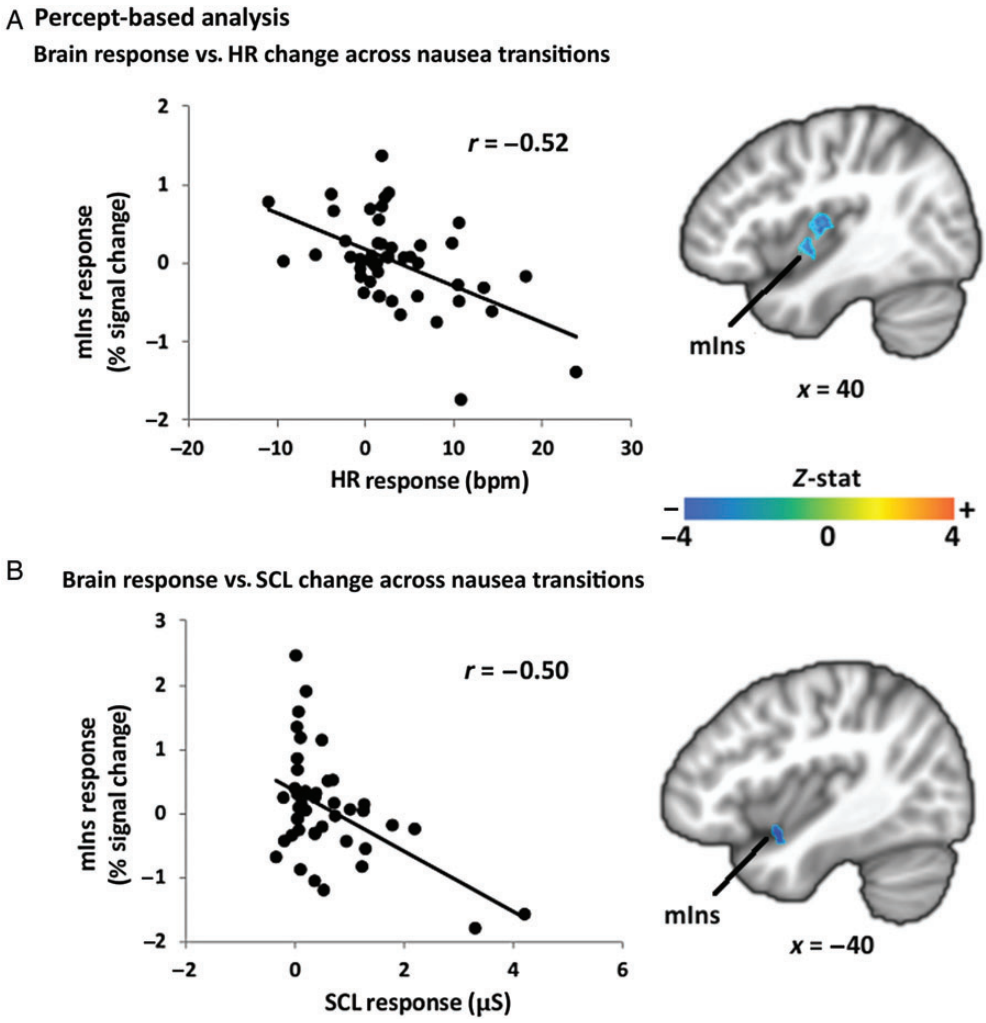

Figure 7. Percept-based analysis: inter-individual correlation between change in mid-insular cortex response and (A) change in HR and (B) change in SCL for increasing nausea sensation. Note: r = Pearson's correlation coefficient; r^* = −0.25, Pearson's correlation coefficient removing the outliers (4.21; −1.58) and (3.30; −1.80), as determined by Grubb's test for outliers.

Table 4
Percept-based analysis: inter-individual correlation between change in brain response and change in ANS response

Brain region	Side	Location (MNI)			*Z*-score
		x	*y*	*z*	
HR					
mIns	R	34	−10	10	−4.4
AnG	L	−40	−50	50	−3.82
LTC	L	−50	12	−18	−3.41
		−52	−22	12	−3.7
	R	58	−38	−10	−3.65
MT + /V5	L	−38	−62	18	−4.26
SCL					
mIns	L	−48	6	−12	−3.67
Cerebellum	L	−22	−82	−18	−3.22

during RECOVERY. This lack of correlation suggests independent processes in ANS response associated with sympathetic and parasympathetic modulation during nausea. Hence, the independence between sympathetic and parasympathetic responses to motion sickness necessitates the monitoring of both ANS divisions when investigating the complex phenomenon of nausea.

Several limitations to our study should be noted. First, while significance was noted for many of the autonomic changes evaluated with our percept- and stimulus-based analyses, there was a lack of significance for some of the more highly variable autonomic indices (e.g. HF-HRV) in our percept-based analysis. This may have been due to insufficient sample size for this combination of analysis method and autonomic index. In addition, we were not able to demonstrate significant autonomic-associated activity in the brainstem. Many autonomic processing nuclei are known to exist in medullary, pontine, and mesencephalic regions, and future studies should adopt specific neuroimaging methods (e.g. higher field strength and smaller voxel size) that focus on brainstem activity in relation to nausea-induced autonomic change. Another limitation was that SCL is known to be an indirect measure of sympathetic activity and is certainly delayed with respect to central signaling of peripheral sympathetic response (Boucsein 2012). Future studies could consider the recovery of the underlying nerve activity relative to the SCL signal, in order to improve the accuracy of modeling for combined ANS/fMRI analyses. As a final note, a recent study showed that magnetic fields associated with the MRI environment produce nystagmus, reportedly interacting with ionic currents in the labyrinthine endolymph fluid, resulting in magnetic vestibular stimulation (Roberts et al. 2011). While our study was performed at 1.5 T and it is unlikely that magnetic field vestibular stimulation influenced the present results (Roberts et al. found much greater effects at 7 T compared with 3 T), future studies should consider this potential confound when choosing MRI field strength.

In conclusion, we found that the increased sympathetic and decreased parasympathetic modulation caused by nausea was associated with a broad central autonomic network including brain regions such as the insula. Specificity in brain activity supporting parasympathetic versus sympathetic modulation was also noted. Activity in default mode network regions and brain regions processing visual motion were most strongly associated with parasympathetic outflow, which was maximally decreased at peak nausea perception. In contrast, brain regions such as the lateral prefrontal cortex were most strongly associated with sympathetic outflow, which was maximally increased after cessation of the nauseogenic stimulation, when subjects were still nauseous but in recovery. These results suggest divergent central autonomic control for sympathetic and parasympathetic response to nausea, while highlighting the role of the insula in mediating both phasic and sustained autonomic response during nausea.

Funding

This work was supported by the National Institutes of Health (grant numbers P01-AT006663, R01-AT007550, and R01-AR064367 to VN, K23-DK069614 to BK, and R21-AR057920 to VN, BK and RB); the National Center for Research Resources (P41RR14075; CRC 1 UL1 RR025758, Harvard Clinical and Translational Science Center); the MGH Department of Anesthesia, Critical Care and Pain Medicine and the International Foundation of Functional Gastrointestinal Disorders.

Notes

The content is solely the responsibility of the authors and does not necessarily represent the official views of our sponsors.

References

Barbieri R, Matten EC, Alabi AA, Brown EN. 2005. A point-process model of human heartbeat intervals: new definitions of heart rate and heart rate variability. Am J Physiol Heart Circulat Physiol. 288(1):H424–H435.

Becker-Bense S, Buchholz H, zu Eulenburg P, Best C, Bartenstein P, Schreckenberger M, Dieterich M. 2012. Ventral and dorsal streams processing visual motion perception (FDG-PET study). BMC Neurosci. 13(1):81.

Beckmann CF, Jenkinson M, Smith SM. 2003. General multilevel linear modeling for group analysis in FMRI. Neuroimage. 20(2): 1052–1063.

Beissner F, Meissner K, Bär K, Napadow V. 2013. The autonomic brain: an activation likelihood estimation meta-analysis for central processing of autonomic function. J Neurosci. 33(25):10503–10511.

Boucsein W. 2012. Electrodermal activity. New York: Springer.

Brooks JC, Faull OK, Pattinson KT, Jenkinson M. 2013. Physiological noise in brainstem fMRI. Front Hum Neurosci 7(623).

Chang C, Cunningham JP, Glover GH. 2009. Influence of heart rate on the BOLD signal: The cardiac response function. Neuroimage. 44(3):857.

Cowings PS, Suter S, Toscano WB, Kamiya J, Naifeh K. 1986. General autonomic components of motion sickness. Psychophysiology. 23 (5):542–551.

Craig AD. 2002. How do you feel? interoception: the sense of the physiological condition of the body. Nat Rev Neurosci 3(8):655–666.

Critchley HD, Wiens S, Rotshtein P, Öhman A, Dolan RJ. 2004. Neural systems supporting interoceptive awareness. Nat Neurosci. 7(2):189–195.

de Haan EH, Cowey A. 2011. On the usefulness of 'what'and 'where'-pathways in vision. Trends Cogn Sci. 15(10):460–466.

Doweck I, Gordon CR, Shlitner A, Spitzer O, Gonen A, Binah O, Melamed Y, Shupak A. 1997. Alterations in R–R variability associated with experimental motion sickness. J Auton Nerv Syst. 67(1):31–37.

Golding JF. 1998. Motion sickness susceptibility questionnaire revised and its relationship to other forms of sickness. Brain Res Bull. 47(5):507–516.

Gray MA, Minati L, Harrison NA, Gianaros PJ, Napadow V, Critchley HD. 2009. Physiological recordings: basic concepts and implementation during functional magnetic resonance imaging. Neuroimage. 47(3):1105–1115.

Graybiel A, Lackner JR. 1980. Evaluation of the relationship between motion sickness symptomatology and blood pressure, heart rate and body temperature. Aviat Space Environ Med. 51(3):211–214.
Ishii M, Igarashi M, Patel S, Himi T, Kulecz W. 1987. Autonomic effects on RR variations of the heart rate in the squirrel monkey: an indicator of autonomic imbalance in conflict sickness. Am J Otolaryngol. 8(3):144.
Jänig W. 2006. The integrative action of the autonomic nervous system: neurobiology of homeostasis. New York: Cambridge University Press, Cambridge.
Kim YY, Kim HJ, Kim EN, Ko HD, Kim HT. 2005. Characteristic changes in the physiological components of cybersickness. Psychophysiology. 42(5):616–625.
LaCount LT, Barbieri R, Park K, Kim J, Brown EN, Kuo B, Napadow V. 2011. Static and dynamic autonomic response with increasing nausea perception. Aviat Space Environ Med. 82(4):424.
Lang PJ. 1994. The varieties of emotional experience: a meditation on James-Lange theory. Pshychol Rev. 101(2):211–221.
Levine ME, Stern RM, Koch KL. 2006. The effects of manipulating expectations through placebo and nocebo administration on gastric tachyarrhythmia and motion-induced nausea. Psychosom Med. 68(3):478–486.
Lin C, Jung T, Chuang S, Duann J, Lin C, Chiu T. 2013. Self-adjustments may account for the contradictory correlations between HRV and motion-sickness severity. Int J Psychophysiol. 87(1):70–80.
Lin Chin-Teng, Lin Chun-Ling, Chiu Tzai-Wen, Duann Jeng-Ren, Jung Tzyy-Ping. 2011. Effect of respiratory modulation on relationship between heart rate variability and motion sickness. Engineering in medicine and biology society, EMBC, 2011 annual international conference of the IEEE. Boston, MA: IEEE. p. 1921.
Lobel E, Kleine JF, Bihan DL, Leroy-WIllig A, Berthoz A. 1998. Functional MRI of galvanic vestibular stimulation. J Neurophysiol. 80(5):2699–2709.
Macefield VG, James C, Henderson LA. 2013. Identification of sites of sympathetic outflow at rest and during emotional arousal: concurrent recordings of sympathetic nerve activity and fMRI of the brain. Int J Psychophysiol. 89(3):451–459.
Mayer E, Aziz Q, Coen S, Kern M, Labus J, Lane R, Kuo B, Naliboff B, Tracey I. 2009. Brain imaging approaches to the study of functional GI disorders: a Rome working team report. Neurogastroenterol Motility. 21(6):579–596.
McClure JA, Fregly AR, Molina E, Graybiel A. 1971. Response from arousal and thermal sweat areas during motion sickness. Naval Aerospace Medical Research Lab, Pensacola (FL), USA. No. NARML-1142.
Money KE. 1970. Motion sickness. Physiol Rev. 50(1):1–39.
Mullen TJ, Berger RD, Oman CM, Cohen RJ. 1998. Human heart rate variability relation is unchanged during motion sickness. J Vestib Res. 8(1):95–105.
Muth ER. 2006. Motion and space sickness: intestinal and autonomic correlates. Autonomic Neurosci. 129(1):58–66.
Muth ER, Stern RM, Thayer JF, Koch KL. 1996. Assessment of the multiple dimensions of nausea: the nausea profile (NP). J Psychosom Res. 40(5):511–520.
Napadow V, Li A, Loggia ML, Kim J, Schalock PC, Lerner E, Tran T, Ring J, Rosen BR, Kaptchuk TJ. 2012. The brain circuitry mediating antipruritic effects of acupuncture. Cerebral Cortex. 24 (4):873–882.
Napadow V, Sheehan JD, Kim J, LaCount LT, Park K, Kaptchuk TJ, Rosen BR, Kuo B. 2013. The brain circuitry underlying the temporal evolution of nausea in humans. Cerebral Cortex. 23 (4):806–813.
Ohyama S, Nishiike S, Watanabe H, Matsuoka K, Akizuki H, Takeda N, Harada T. 2007. Autonomic responses during motion sickness induced by virtual reality. Auris Nasus Larynx. 34(3):303–306.
Oldfield RC. 1971. The assessment and analysis of handedness: the edinburgh inventory. Neuropsychologia. 9(1):97–113.
Roberts DC, Marcelli V, Gillen JS, Carey JP, Della Santina CC, Zee DS. 2011. MRI magnetic field stimulates rotational sensors of the brain. Current Biology. 21(19):1635–1640.
Saper CB. 2002. The central autonomic nervous system: conscious visceral perception and autonomic pattern generation. Annu Rev Neurosci. 25(1):433–469.
Sheehan SE, Oman CM, Duda KR. 2011. Motion sickness: a cholinomimetic agent hypothesis. J Vestib Res. 21(4):209–217.
Shoemaker JK, Wong SW, Cechetto DF. 2012. Cortical circuitry associated with reflex cardiovascular control in humans: Does the cortical autonomic network "speak" or "listen" during cardiovascular arousal. Anat Rec. 295(9):1375–1384.
Stern RM. 2002. The psychophysiology of nausea. Acta Biologica Hungarica. 53(4):589–600.
Stern RM, Koch KL, Andrews PL. 2011. Nausea: Mechanisms and management. New York: Oxford University Press.
Thayer JF, Åhs F, Fredrikson M, Sollers III JJ, Wager TD. 2012. A meta-analysis of heart rate variability and neuroimaging studies: Implications for heart rate variability as a marker of stress and health. Neurosci Biobehav Rev. 36(2):747–756.
Wiens S. 2005. Interoception in emotional experience. Curr Opin Neurol. 18(4):442.
Wiggins G, Triantafyllou C, Potthast A, Reykowski A, Nittka M, Wald L. 2006. 32-channel 3 tesla receive-only phased-array head coil with soccer-ball element geometry. Magn Reson Med. 56 (1):216–223.
Yokota Y, Aoki M, Mizuta K, Ito Y, Isu N. 2005. Motion sickness susceptibility associated with visually induced postural instability and cardiac autonomic responses in healthy subjects. Acta Otolaryngol. 125(3):280–285.